



Comparative Study of Corrosion Behaviour of Martensitic and Supermartensitic Stainless Steels in Two Corrosive Media

Amel Oulabbas^{1,2*}, Samira Tlili¹ and Soumaya Meddah¹

¹Research Center In industrial technologies CRTI P.O.Box 64, Cheraga 16014 Algiers, (Algeria).

²Laboratoire d'Ingénierie des Surfaces (LIS), Université Badji Mokhtar- Annaba (Algérie).

(Corresponding author: Amel Oulabbas*)

(Received 05 May 2021, Revised 23 July 2021, Accepted 25 August 2021)

(Published by Research Trend, Website: www.researchtrend.net)

ABSTRACT: Supermartensitic stainless steels deduced from the refinement of the composition of martensitic steels, have a low carbon content with 13% chromium, 5% nickel and 2% molybdenum, this new generation of steel has an improved ductility with good mechanical strength and excellent corrosion resistance. The objective of this paper is to prove this resistance to hydrogen diffusion in the austenitic phase, and to study the resistance to sulfate corrosion and chloride pitting. The corrosion properties will be discussed in relation to their metallurgical microstructure. Stationary (polarization curves) and transient (electrochemical impedance) electrochemical methods were applied. The corrosion rate as a function of time was determined by the mass loss method and the characterization of the surface state was studied by optical microscopy. Two types of corrosion were observed: a uniform corrosion in which the half-reactions are homogeneously distributed in 0.5M H₂SO₄, followed by a localized corrosion observed in 0.5M NaCl for both steels. According to the polarization curves, the corrosion potential differs between martensitic and supermartensitic steel where it shows a higher potential with -0.342V/Ag/AgCl in 0.5M H₂SO₄ and -0.339 V/Ag/AgCl in 0.5M NaCl. In parallel, the polarization resistance given by EIS shows that in both media, supermartensitic steel is more resistant than martensitic steel where it has an Rp equal to 7200 Ohm in 0.5M H₂SO₄ and 8340 Ohm 0.5M NaCl. These results are confirmed by the optical microscope images.

Keywords: Martensitic steel, supermartensitic steel, electrochemical impedance, corrosion.

I. INTRODUCTION

In the oil industry (oilfields and marine environment applications), steel is widely used [1], but the replacement of carbon steels started in the 1970s by martensitic stainless steels due to their affordability and better corrosion resistance compared to most of the materials used [2, 3]. In order to improve the weldability factor and to have a better corrosion resistance, the composition of martensitic steels has been refined in recent years, with a reduction of the carbon content [4] and then the addition of elements promoting the presence of the austenitic phase after welding, which improves the toughness of these welded joints [5]. This new generation of steel is called supermartensitic [6]. These steels combine good weldability and strength with excellent corrosion resistance. This name was given to them because their microstructure is mainly composed of adiabatic martensite. Its formation depends only on the temperature reached below the martensitic transformation starting temperature (Ms) and not on the cooling rate obtained to reach Ms [7]. The martensite of conventional martensitic steels is not adiabatic, this is the main difference with supermartensitic steels.

Supermartensitic steels contain many alloying elements that have the effect of lowering Ms [8].

Essentially, supermartensitic stainless steels are chromium (Cr), nickel (Ni) and molybdenum (Mo) based steels with a low concentration of carbon (C). Chromium is an important element for corrosion resistance and the addition of nickel and molybdenum is mainly used to compensate for the decrease in carbon to promote austenite formation [9]. This allows them to retain good strength, like conventional martensitic steels such as

AISI 410 and low cost compared to duplex steels with higher chromium content [10, 11]. Molybdenum, Mo, like copper, improves corrosion resistance in most corrosive environments, especially acidic ones, but also in phosphoric solutions, sulfur, etc. It increases the stability of passivation films and is mainly added to control carbide embrittlement of the alloy after the martensite tempering treatment [12].

martensite [12]. In this work, we studied the behavior of these two stainless steels, martensitic and supermartensitic, in a sulfide medium and another chloride medium. In the same vein, Kimura *et al.*, [13]. The impact of residual austenite on corrosion rate and pitting susceptibility was studied. These authors found that residual austenite had a slightly positive effect on corrosion resistance. They explain these results by the fact that hydrogen diffuses more rapidly into martensite. This was confirmed just after in 2020 [14]. The complex metallurgical structure of martensitic stainless steel causes failures in the industry such as sulfide stress cracking and intergranular corrosion [15], hence the limitation of using this martensitic grade.

In the first part, we used the mass loss method to evaluate the degree of degradation by estimating the corrosion rate. In the second part, we performed the electrochemical study by describing the attack mechanism at the metal/electrolyte interface.

II. MATERIALS AND METHODS

The variation of the corrosion rate has been studied using the mass loss test, which is a first approach to the corrosion of a metal immersed in an electrolyte in order to determine their corrosion rate as a function of time [16]. Mass loss measurements are performed at

different immersion times and at an ambient temperature of 25 °C [17].

Two samples, one of which is a martensitic steel and the other a supermartensitic steel, were prepared and weighed prior to analysis and before immersion in 0.5M H₂SO₄ and 0.5M NaCl, respectively, to study the evolution of the corrosion rate as a function of time, from 24hr to 420hr. The mass loss test gives a direct estimate of the corrosion rate of the steel immersed in the electrolyte [18, 19]. The corrosion rate is calculated by the following formula:

$$V = \Delta M / S \cdot t \text{ (mg/h.cm}^2\text{)} \quad (1)$$

With: $\Delta M = M1 - M2$

ΔM is the difference between the initial mass $M1$ and the final mass $M2$ after a time t . S is the surface of the metal exposed to the electrolyte. Once the surfaces of the samples are polished, the initial masses of each sample immersed in the solution are measured in 25ml of 0.5M H₂SO₄ and 25ml of 0.5 M NaCl separately in covered beakers at a temperature of 25 °C. After each immersion time, the samples are rinsed with distilled water, brushed with acetone and dried with an electric dryer. Finally, the mass $M2$ is weighed.

This technique gives us the values of the corrosion potential and allows us to access the values of the corrosion current density (Tafel's law) thanks to which we can calculate the corrosion rate. The curves are plotted by the Autolab 302 corrosion chain, the scan was performed at a speed of 60mV/min between 1 mV/Ag/AgCl. It should be noted that for all the tests, a waiting period of 1h after immersion corresponding to

the time of formation and stability of the electrical double layer was respected.

Throughout the study, the impedance measurements were performed in potentiostatic mode around the polarization point E_{corr} , with a sinusoidal perturbation equal to 5mV, knowing that the frequencies swept during the impedance measurements are between 100 kHz and 10 mHz.

In order to highlight and compare the surface microstructure of martensitic and super martensitic steels, this method of metallography of well polished surfaces before and after electrolytic etching is used. We used a NIKON ECLIPSELV 100 ND optical microscope equipped with 50, 100, 200 and 500 times magnification lenses. The micrographs are acquired with a video camera attached to the microscope and connected to a computer.

In order to study and visualize closely the morphological change of the surface of martensitic and supermartensitic steels exposed to electrolytes, the samples were immersed in the electrolytes for one hour. They were then rinsed with distilled water and dried immediately with a dryer. SEM images were taken with a ZEISS-EVO/MA25.

III. RESULTS AND DISCUSSION

A. Weight loss

Table 1 shows the corrosion rate results for the two steels in the two corrosive environments, calculated by equation (1).

Table 1: Variation of the corrosion rate of the two steels in 0.5M H₂SO₄ and 0.5M NaCl.

Immersion time (h)	0.5M H ₂ SO ₄		0.5M NaCl	
	V (g/m ² .h)		V (g/m ² .h)	
	Martensitic stainless steel	Supermartensitic stainless steel	Martensitic stainless steel	Supermartensitic stainless steel
0	/	/	/	/
24	0.0041	0	0.0041	0
48	0.0045	0.0020	0.0062	0.0020
72	0.0055	0.0027	0.0069	0.0021
96	0.0072	0.0031	0.0083	0.0032
120	0.0083	0.0033	0.0091	0.0034
420	0.0088	0.0035	0.0092	0.00047

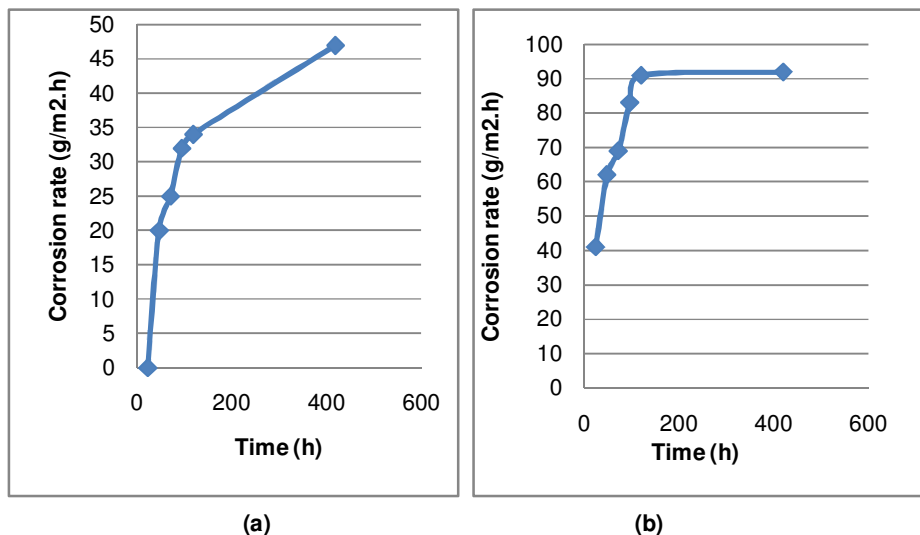


Fig. 1. Variation in corrosion rate with time (a) martensitic steel et (b) : supermartensitic steel in 0.5M H₂SO₄.

In both environments, H₂SO₄ and chloride, the corrosion rate is higher for martensitic steel than for supermartensitic steel, it increases with time, which translates into an aggression of the metal by the rapid diffusion of sulfate ions in H₂SO₄ 0.5 M and by Cl⁻ ions in NaCl 0.5M. At a time equal to 420h this speed decreases, which translates the presence of a barrier at the surface of the metal, which lets believe that there is a protection whereas the corrosion is camouflaged and always deteriorates the two steels by oxidation of iron under this barrier.

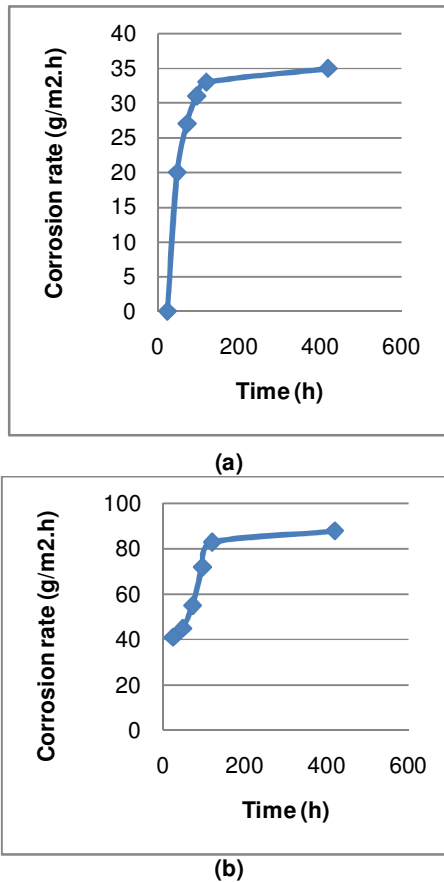


Fig. 2. Variation in corrosion rate with time for: (a): martensitic stainless steel and (b): supermartensitic stainless steel steel in 0.5M NaCl

In general, the anodic and cathodic reactions of an iron alloy (carbon steel) in an aerated neutral solution are
 -Cathodic reaction: $O_2 + 2 H_2O + 4 e^- \rightarrow 4OH^-$ (1)
 -Anodic reaction: $Fe \rightarrow Fe^{2+} + 2e^-$ (2)
 $Fe^{2+} + 2OH^- \rightarrow Fe(OH)_2$ (3)

The diagrams presented in Fig. (1) in a sulfated environment show that the corrosion rate increases with time. In the case of martensitic steel at (t120h) where the rate reaches 0.0083g/m².h, a slowdown of the latter is observed until stabilization. This reflects the presence of a protective film that covers the entire surface of the steel. For supermartensitic steel, the values of the corrosion rate in sulfate medium are very low and reach their maximum values at t120. These negligible values show the high corrosion resistance of this steel compared to martensitic steel. The same is true for the chloride medium where the corrosion rate values between the two steels are different, the supermartensitic steel having a high resistance to polarization even with the attack of Cl⁻ ions.

A. Electrochemical measurements

(i) Potentiodynamic curves. The results of the various electrochemical tests of the two martensitic and supermartensitic steels respectively in 0.5M NaCl and 0.5M H₂SO₄ are shown in Fig. 3 and 4.

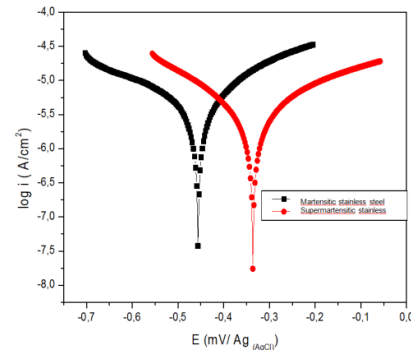


Fig. 3. Polarisation curves of martensitic and supermartensitic stainless steel in 0.5M NaCl.

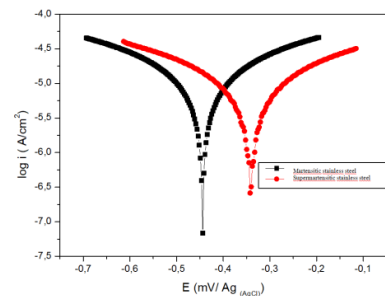


Fig. 4. Polarisation curves of martensitic and supermartensitic stainless steel in 0.5M H₂SO₄.

characterized by the oxidation of iron and the reduction of oxygen dissolved in the medium according to:

Tables 2 and 3 combine the results of the Tafel curves of the two steels studied in 0.5M NaCl and 0.5M H₂SO₄:

Table 2: Electrochemical parameters deduced from polarisation curves in 0.5M NaCl.

	E _{corr} (mV)	I _{corr} (mA/cm ²)	β _a (mV)	β _c (mV)
Martensitic stainless steel	-464.5	0.043	58.6	170.9
Supermartensitic stainless steel	-328.2	0.027	84.9	121.4

Table 3: Electrochemical parameters deduced from polarisation curves in 0.5M H₂SO₄.

	E _{corr} (mV)	I _{corr} (mA/cm ²)	Ba (mV)	Bc (mV)
Martensitic stainless steel	-456.5	0.058	69.6.6	132.7
Supermartensitic stainless steel	-335.2	0.015	71.5	116.2

Examination of the polarization curves obtained for the steels immersed in 0.5 M NaCl, shows that the corrosion potential of the supermartensitic steel tends towards more positive values with 328.2 mV compared to the electrode potential of 464.5 mV of the martensitic steel, at the same time a decrease in the current density for the anodic branch due to the dissolution of iron. The same behavior is noticed in the medium H₂SO₄ at 0.5 M, the reduction of current densities up to 0.015 mA/cm² and the onction of potentials for supermartensitic steel at 335.2 mV where the dissolution of iron is less rapid because it is blocked by the oxides of chromes that form a protective surface film of the metal [20-22]. These results explain the results found with the mass loss technique and confirm the presence of an anti-corrosive layer of the metal interface for supermartensitic steel.

(ii) **Electrochemical impedance spectroscopy.** Impedance measurements were carried out under the same conditions on two working electrodes, martensitic and supermartensitic steels, in two different environments.

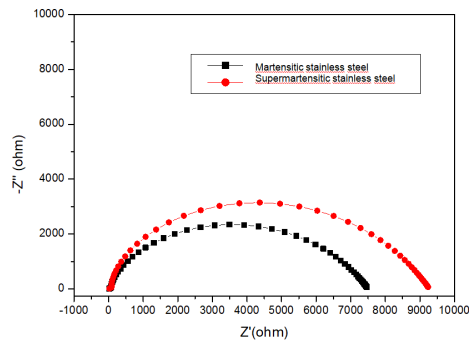


Fig. 5. Electrochemical impedance diagrams (Nyquist representation) of Martensitic and super martensitic Stainless steel in 0.5M NaCl.

The EIS diagrams obtained on the substrates immersed in NaCl showed at least the presence of two time constants. Indeed, the weak capacitive HF loop leads us to believe that it is simply due to a parasitic or additional process of the electronic interface (negligible current, cable resistance, distances between electrodes).

The HF capacitive loop is attributed to the corrosion process taking place at the electrochemical interface

Table 1: Impedance parameters of martensitic and supermartensitic stainless steel in 0.5 M NaCl.

	R _e (Ω)	CPE _{dl} (F.S ^{1/n})	n _{dl}	R _{ct} (Ω)	CPE _c (F.S ^{1/n})	n _c	R _c (Ω)
Martensitique stainless steel	8.03	8.54 10 ⁻⁶	0.7	154	214 10 ⁻⁹	0.9	7.35 10 ⁺³
super martensitique stainless steel	6.96	5.96 10 ⁻⁶	0.7	140	102.10 ⁻⁹	0.9	9.13 10 ⁺³

characterized by a constant phase element Cpedl in parallel with the charge transfer resistance Rct [23].

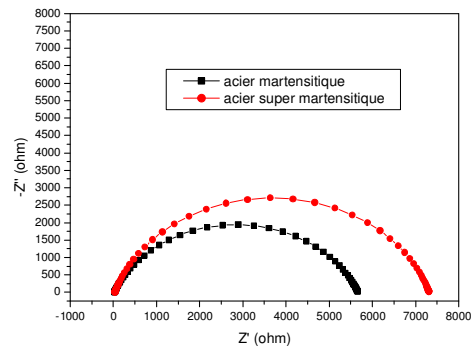


Fig. 6. Electrochemical impedance diagrams (Nyquist representation) of Martensitic and super martensitic Stainless steel in 0.5M H₂SO₄.

Indeed, the presence of chromium in the composition of both substrates, together with molybdenum and nickel, stimulates the spontaneous formation of oxides and spinels by combining with Fe²⁺ from the dissolution of the substrate. For supermartensitic steel, the size of the capacitance loop is larger compared to martensitic steel, resulting in a higher polarization resistance, and according to Table 1, it is 9130 Ohm, while it is around 7350 Ohm for martensitic steel. The EPC capacitance values, which decrease with supermartensitic steel, confirm these results with a value equal to 102.10⁻⁹ F.S^{1/n}.

For martensitic and supermartensitic steel immersed in 0.5M H₂SO₄, after 1 hour of immersion of the substrates, corrosion products are deposited on the surface of the metal. It is assumed that nickel sulfides, which are inhibitors of hydrogen recombination, are present in the sulfated medium, showing a beneficial effect that reduces in particular the defects of the passive film. The charge transfer strength of the supermartensitic steel is higher with 5970 Ohm and a lower capacitance than for the martensitic steel, which is equal to 115 10⁻⁹ F.S^{1/n}. Similar values of CPE_c have already been reported for a Fe17Cr stainless steel [24].

Table 4 and 5, group together the electrochemical parameters derived from the Nyquist diagrams, in 0.5M NaCl and 0.5M H₂SO₄ respectively.

Table 2: Impedance parameters of martensitic and supermartensitic stainless steel in 0.5 M H₂SO₄

	R_e (Ω)	CPE_{dl} ($F.S^{1/n}$)	n_{dl}	R_{ct} (Ω)	CPE_c (F.S ^{1/m})	n_c	R_c (Ω)
Martensitique stainless steel	23.5	$6.07 \cdot 10^{-6}$	0.7	694	$12.5 \cdot 10^{-6}$	0.9	$4.98 \cdot 10^{-3}$
super martensitique stainless steel	34.3	$3.97 \cdot 10^{-6}$	0.8	$1.31 \cdot 10^{-3}$	$115 \cdot 10^{-9}$	0.9	$5.97 \cdot 10^{-3}$

For corrosion in a saline environment, the electrochemical kinetics are rapid in the moments following immersion, then slowed down by the appearance and growth of corrosion products. The modeling of these systems is therefore not easy and must take into account the permanent reduction of the surface.

Many authors have tried to characterize the corrosion of steel in different electrolytes, in this case H₂SO₄ [7], Na₂SO₄ [9], NaCl saturated with H₂S, by EIS measurements. No universal model has been proposed for the corrosion of martensitic and supermartensitic steels.

The model describing the electrochemical behavior of the stainless steel-solution interface in NaCl during the formation of the corrosion product layer is schematically as follows:

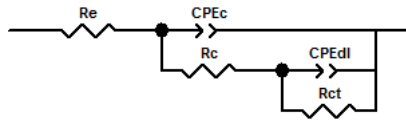


Fig. 7. Equivalent circuit of stainless steel immersed in NaCl

Thus, the proposed equivalent circuit, giving the response of the electrochemical interface relative to the substrate immersed in H₂SO₄ is as follows:

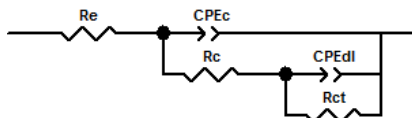


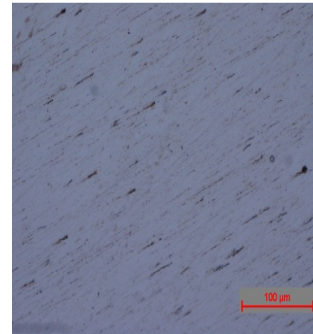
Fig. 8. Equivalent circuit of stainless steel immersed in H₂SO₄

C. Characterization of surface by optic spectroscopy

The surface condition after corrosion tests in different media for the two steels studied is presented in Figures 5 and 6. The surfaces of the samples were observed by optical microscopy after 1 hour of immersion for both steel samples and in both electrolytes. It was found that corrosion develops after immersion in both aggressive media. The images clearly show the difference in Cl⁻ and SO₄²⁻ attack, which can be seen by the density and size of the corrosion defects increasing more in the chloride medium than in the sulfate medium. It is therefore clear that supermartensitic steel is more resistant than martensitic steel in both media, which confirms the results obtained by the mass loss and polarization curve.

D. Characterization of surface by electron microscopy (SEM)

The micrographs of the two martensitic and supermartensitic steels immersed in H₂SO₄ and immersed in NaCl are in Fig. 7.



(a)



(b)

Fig. 9. Optic spectroscopy Micrography of (a) martensitic and (b) supermartensitic stainless steel before and after immersion in 0.5 M NaCl.



(a)



(b)

Fig. 10. Optic spectroscopy Micrography of (a) martensitic and (b) supermartensitic stainless steel before and after immersion in 0.5 M H₂SO₄.

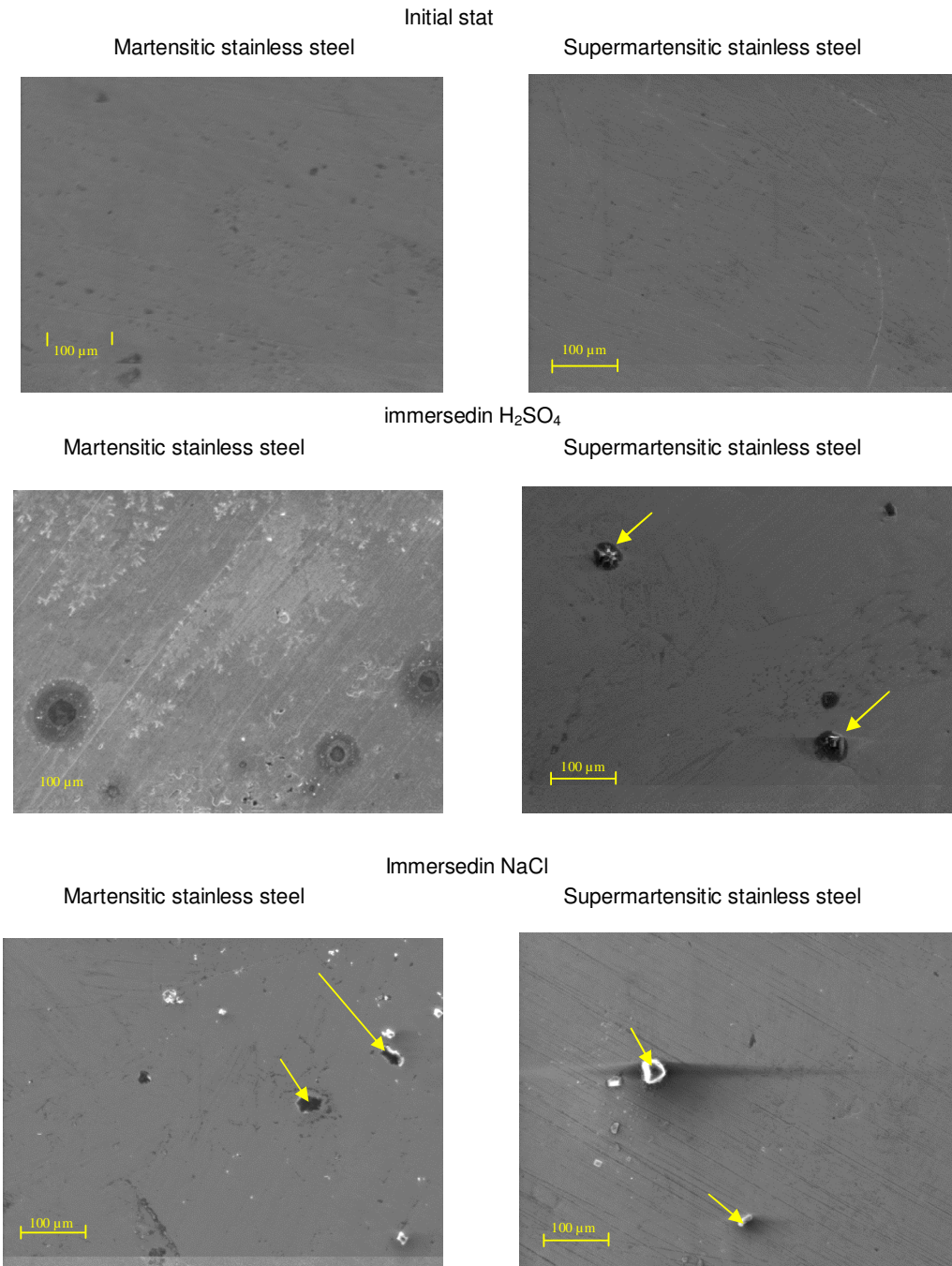


Fig. 11. SEM micrographs of supermartensitic and martensitic stainless steel in NaCl and H₂SO₄ media.

First and foremost and in a sulfate environment, the surface of martensitic steel clearly shows a significant degradation of the surface compared to the initial state of martensitic steel, with the presence of crevice corrosion sites that have the appearance of enlarged tips. Compared to supermartensitic steel where the attack results in the presence of deposits of corrosion products on the surface and whose degradation is less significant.

Secondly, in the case of stainless steels immersed in the chloride medium, pitting corrosion in both cases is due to the attack of Cl ions, and obviously the number of pits is higher in the case of martensitic steel, which is well known for martensitic stainless steels in neutral medium [25-30]. These results are in good agreement with what has been discussed and found, with the previous methods (weight loss and electrochemical).

IV. CONCLUSION

The main objective of this work is to compare the corrosion behavior from the martensitic and supermartensitic point of view. The conclusions that can be drawn are the following:

- From the mass loss technique, we obtained a difference in corrosion rates that favors the supermartensitic steel.
- The polarization curves (Tafel) show that the corrosion potentials are different. The dropout potential of the supermartensitic steel is more noble than that of the martensitic steel. Thus the current intensities are lower in the case of supermartensitic steel.
- Optical microscope characterization of the surface confirms these results.
- Nyquist diagrams show higher polarization strengths in the case of supermartensitic steel.
- The EPC values decrease with supermartensitic steel reflecting the good corrosion resistance.
- SEM micrographs of martensitic steel in both study media clearly show that the corrosion process is more apparent compared to supermartensitic steel.

V. FUTURE SCOPE

- These surface characterization methods are in addition to the methods previously carried out in the literature that study the mechanical and structural properties of supermartensitic steel to clearly show the strength of super martensitic steel.
- The study of the microstructure, wear and corrosion resistance of supermartensitic stainless steel (SMSS) is yet to be explored in other corrosive environments such as seawater and acidic environment.

Acknowledgements

The authors would like to thank the Industrial Technology Research Center CRTI for the financial and technical support of this project. And would also like to thank the Directorate General of Scientific Research and Technological Development

REFERENCES

- [1]. Nazir, A., & Lal, H. (2015). Utilisation des déchets en préparant le produit du forgeage des copeaux d'acier allié (16MNCr5). *Revue internationale sur les technologies émergentes*, 6 (2), 181.
- [2]. Li, CX et Bell, T. (2006). Propriétés de corrosion de l'acier inoxydable martensitique AISI 410 nitruré au plasma dans des solutions aqueuses à 3,5 % de NaCl et 1 % de HCl. *Science de la corrosion*, 48 (8), 2036-2049.
- [3]. Isfahany, AN, Saghafian, H., & Borhani, G. (2011). L'effet du traitement thermique sur les propriétés mécaniques et le comportement à la corrosion de l'acier inoxydable martensitique AISI420. *Journal des alliages et composés*, 509 (9), 3931-3936.
- [4]. Wang, P., Lu, SP, Xiao, NM, Li, DZ et Li, YY (2010). Effet de la ferrite delta sur les propriétés d'impact de l'acier inoxydable martensitique 13Cr-4Ni à faible teneur en carbone. *Science et génie des matériaux : A*, 527 (13-14), 3210-3216.
- [5]. Kvaale, P. E., & Olsen, S. (1999). Experience with supermartensitic stainless steels in flowline applications. *Stainless Steel World*, 99, 19-26.
- [6]. Zou, DN, Han, Y., Zhang, W. et Fang, XD (2010). Influence du processus de revenu sur les propriétés mécaniques de l'acier inoxydable

supermartensitique 00Cr13Ni4Mo. *Journal of Iron and Steel Research International*, 17 (8), 50-54.

- [7]. Koistinen, D. P. (1959). A general equation prescribing the extent of the austenite-martensite transformation in pure iron-carbon alloys and plain carbon steels. *acta metallurgica*, 7, 59-60.
- [8]. Dufrane, J. J. (1999). Metallurgical basis for the development of weldable martensitic stainless steels. *Supermartensitic Stainless Steels*, 99, 19-24.
- [9]. Bojack, A., Zhao, L., Morris, PF et Sietsma, J. (2012). Détermination in situ de la formation d'austénite et de martensite dans l'acier inoxydable supermartensitique 13Cr6Ni2Mo. *Caractérisation des matériaux*, 71 : 77-86.
- [10]. Smith, L. M., & Celant, M. (1999). Martensitic stainless steel flowlines—Do they pay. *Supermartensitic Stainl. Steels*, 1999, 66-73.
- [11]. Ahn, S. H., Plancarte, J., & Wright, P. K. (2000). The Impact of Reference Free Part Encapsulation (RFPE) on Design for Manufacturability with CNC Machining. In *International Design Engineering Technical Conferences and Computers and Information in Engineering Conference* (Vol. 35135, pp. 251-259). American Society of Mechanical Engineers.
- [12]. Iwabuchi, Y., & Sawada, S. (1982). Caractéristiques métallurgiques d'une grande coulée hydraulique en acier inoxydable de type 13Cr-Ni. En *moulages d'acier inoxydable*. ASTM International.
- [13]. Kimura, M., Miyata, Y., Toyooka, T., & Kitahaba, Y. (2000, mars). Effet de l'austénite retenue sur les performances de corrosion pour les tuyaux en acier modifiés à 13 % Cr. Dans *CORROSION 2000*. OnePetro.
- [14]. He, J., Chen, L., Tao, X., Antonov, S., Zhong, Y., & Su, Y. (2020). Comportement à la fragilisation par l'hydrogène de l'acier inoxydable supermartensitique 13Cr-5Ni-2Mo. *Science de la corrosion*, 176, 109046.
- [15]. Tavares, S. S. M., Da Silva, F. J., Scandian, C., Da Silva, G. F., & De Abreu, H. F. G. (2010). Microstructure and intergranular corrosion resistance of UNS S17400 (17-4PH) stainless steel. *Corrosion science*, 52(11), 3835-3839.
- [16]. Guillon, E. (2004). *Durabilité des matériaux cimentaires: modélisation de l'influence des équilibres physico-chimiques sur la microstructure et les propriétés mécaniques résiduelles* (Doctoral dissertation, École normale supérieure de Cachan-ENS Cachan).
- [17]. Nedyalkova, I. (2018). *Décontamination des aciers des centrales nucléaires* (Thèse de doctorat, Université de Manchester).
- [18]. Huet, B. (2005). *Comportement à la corrosion des armatures dans un béton carbonaté. Influence de la chimie de la solution interstitielle et d'une barrière de transport* (Doctoral dissertation, INSA Lyon).
- [19]. Aldykiewicz Jr, A. J., Davenport, A. J., & Isaacs, H. S. (1996). Studies of the Formation of Cerium-Rich Protective Films Using X-Ray Absorption Near-Edge Spectroscopy and Rotating Disk Electrode Methods. *Journal of the Electrochemical Society*, 143(1), 147.
- [20]. Marcellin, S., Pèbère, N., & Régnier, S. (2013). Caractérisation électrochimique d'un acier inoxydable martensitique dans une solution de chlorure neutre. *Electrochimica Acta*, 87, 32-40.
- [21]. CAbreu, C. M., Cristóbal, M. J., Losada, R., Nóvoa, X. R., Pena, G., & Pérez, M. C. (2004). High frequency impedance spectroscopy study of passive films formed

on AISI 316 stainless steel in alkaline medium. *Journal of electroanalytical chemistry*, 572(2), 335-345.

[22]. YKim, YP, Fregonese, M., Mazille, H., Feron, D., & Santarini, G. (2006). Etude de la réduction de l'oxygène sur les surfaces en acier inoxydable et de sa contribution aux émissions acoustiques enregistrées lors des processus de corrosion. *Science de la corrosion*, 48 (12), 3945-3959.

[23]. Orazem, ME, Pébère, N., & Tribollet, B. (2006). Représentation graphique améliorée des données d'impédance électrochimique. *Journal de la société électrochimique*, 153 (4), B129.

[24]. Hirschorn, B., Orazem, M. E., Tribollet, B., Vivier, V., Frateur, I., & Musiani, M. (2010). Constant-phase-element behavior caused by resistivity distributions in films: II. Applications. *Journal of The Electrochemical Society*, 157(12), C458.

[25]. Pardo, A., Merino, M. C., Coy, A. E., Viejo, F., Arrabal, R., & Matykina, E. (2008). Effect of Mo and Mn additions on the corrosion behaviour of AISI 304 and 316 stainless steels in H₂SO₄. *Corrosion Science*, 50(3), 780-794.

[26]. Mesquita, T. J., Chauveau, E., Mantel, M., Kinsman, N., & Nogueira, R. P. (2011). Anomalous

corrosion resistance behavior of Mo-containing SS in alkaline media: The role of microstructure. *Materials chemistry and physics*, 126(3), 602-606.

[27]. Mesquita, T. J., Chauveau, E., Mantel, M., Kinsman, N., Roche, V., & Nogueira, R. P. (2012). Lean duplex stainless steels—The role of molybdenum in pitting corrosion of concrete reinforcement studied with industrial and laboratory castings. *Materials Chemistry and Physics*, 132(2-3), 967-972.

[28]. Pardo, A., Merino, M. C., Coy, A. E., Viejo, F., Arrabal, R., & Matykina, E. J. C. S. (2008). Pitting corrosion behaviour of austenitic stainless steels—combining effects of Mn and Mo additions. *Corrosion Science*, 50(6), 1796-1806.

[29]. Mesquita, T., Chauveau, E., Mantel, M., Kinsman, N., & Nogueira, R. P. (2011). Lean duplex stainless steels—The role of molybdenum addition on pitting corrosion of concrete reinforcements. *Revue de Métallurgie*, 108(4), 203-211.

[30]. Mesquita, T. J., Chauveau, E., Mantel, M., & Nogueira, R. P. (2013). A XPS study of the Mo effect on passivation behaviors for highly controlled stainless steels in neutral and alkaline conditions. *Applied surface science*, 270, 90-97.

How to cite this article: Oulabbas, A., Tlili, S. and Meddah, S. (2021). Comparative Study of Corrosion Behaviour of Martensitic and Supermartensitic Stainless Steels in Two Corrosive Media. *International Journal on Emerging Technologies*, 12(2): 269–276.